The Astrophysical Journal, 751:19 (12pp), 2012 May 20 doi:10.1088/0004-637X/751/1/19

WAVELET ANALYSIS AS A TOOL TO LOCALIZE MAGNETIC AND CROSS-HELICITY EVENTS IN THE SOLAR WIND

D. Telloni[1], R. Bruno[2], R. D'Amicis[2], E. Pietropaolo[3], and V. Carbone[4,5]
[1] National Institute for Astrophysics, Astronomical Observatory of Torino, Via Osservatorio 20, 10025 Pino Torinese, Italy
[2] National Institute for Astrophysics, Institute for Interplanetary Space Physics, Via del Fosso del Cavaliere 100, 00133 Roma, Italy
[3] Department of Physics, University of L'Aquila, Via Vetoio Località Coppito, 67100 L'Aquila, Italy
[4] Department of Physics, University of Calabria, Via Ponte P. Bucci Cubo 31/C, 87036 Rende, Italy
[5] National Research Council, Liquid Crystal Laboratory, Via Ponte P. Bucci Cubo 31/C, 87036 Rende, Italy
Received 2011 September 21; accepted 2012 March 13; published 2012 April 30

ABSTRACT

In this paper, we adopt the use of the wavelet transform as a new tool to investigate the time behavior at different scales of reduced magnetic helicity, cross-helicity, and residual energy in space plasmas. The main goal is a better characterization of the fluctuations in which interplanetary flux ropes are embedded. This kind of information is still missing in the present literature, and our tool can represent the basis for a new treatment of in situ measurements of this kind of event. There is a debate about the origins of small-scale flux ropes. It has been suggested that they are formed through magnetic reconnection in the solar wind, such as across the heliospheric current sheet. On the other hand, it has also been suggested that they are formed in the corona, similar to magnetic clouds. Thus, it looks like that there are two populations, one originating in the solar wind via magnetic reconnection across the current sheet in the inner heliosphere and the other originating in the corona. Small-scale flux ropes might be the remnants of the streamer belt blobs formed from disconnection; however, a one-to-one observation of a blob and a small-scale flux rope in the solar wind has yet to be found. Within this panorama of possibilities, this new technique appears to be very promising in investigating the origins of these objects advected by the solar wind.

Key words: interplanetary medium – magnetohydrodynamics (MHD) – methods: data analysis – solar wind

Online-only material: color figures

1. INTRODUCTION

Since the first experimental evidence reported by Coleman in 1968, it has been recognized that fluctuations of characteristic quantities detected in the solar wind can be described within the three-dimensional magnetohydrodynamics (MHD) turbulence, at least for frequencies below the ion-cyclotron frequency, resulting in about 0.1 Hz in solar wind at 1 AU (see Bruno & Carbone 2005 and references therein). However, the solar wind is a dissipationless plasma; that is, at higher frequencies kinetic effects, rather than the usual ∇^2-terms of MHD equations, are responsible for energy dissipation (Matthaeus et al. 2008). The physical processes that replace viscous dissipation in solar wind and the scales where this becomes actively at work have not yet been identified unambiguously, and this remains a matter of strong debate (see the discussion in Bruno & Carbone 2005). Solar wind turbulence is also characterized by the presence of localized coherent structures on all scales, namely, periods where the characteristic time of fluctuations is significantly longer than neighbor fluctuations. These structures are the result of the intermittent process within MHD turbulence. However, long-lived structures can also emerge from the ideal (or quasi-ideal) MHD decay, because ideal MHD is characterized by three rugged invariants, quadratic quantities that are invariant of the dynamics of ideal MHD equations and are insensitive to any truncation of interaction triads in the wavevector space (Woltjer 1958). Apart from the total (magnetic plus kinetic) energy, these quantities are the magnetic helicity and the cross-helicity. Numeric simulations (Ting et al. 1986) and simplified models (Carbone & Veltri 1992) have shown that the dynamic evolution of incompressible MHD is characterized by either a decay toward a maximal magnetic helicity at the largest scale or a maximal cross-helicity on all scales. Intermediate states, if even possible, are rare and are in general due to a lack of resolution. The first case has been viewed as belonging more to laboratory plasmas, the maximal helicity being the result of a selective decay toward a force-free Taylor state (Taylor 1974). The second case, typical of solar wind turbulence within corotating high-speed streams, was predicted by Dobrowolny et al. (1980) as a consequence of the dynamic alignment mechanism. The role of the rugged invariants in solar wind turbulence has been emphasized by Matthaeus & Goldstein (1982). However, investigating the interplay between a given class of large-scale structures and the presence of rugged invariants is useful in disentangling the role played by pseudo-ideal MHD decay and large-scale structure formation in solar wind turbulence.

The magnetic helicity is a measure of the twist or, more generally speaking, of the writhe or flux tube linkage of the magnetic field (Moffat 1978). This physical descriptor of the magnetic field topology is defined as

$$H_m = \int \mathbf{A} \cdot \mathbf{B}\, d^3\mathbf{r}, \tag{1}$$

where $\mathbf{B}(\mathbf{x}, t)$ is the magnetic field strength and $\mathbf{A}(\mathbf{x}, t)$ is the vector potential so that $\mathbf{B} = \nabla \times \mathbf{A}$. The integral is extended over all field-containing regions. The cross-helicity is defined through

$$H_c = \int \mathbf{V} \cdot \mathbf{B}\, d^3\mathbf{r}, \tag{2}$$

where $V(\mathbf{x}, t)$ represents the velocity field. This quantity represents a measure of the magnetic field and velocity fluctuating vectors alignment. From the definitions of both quantities, it can be immediately realized that the information on magnetic helicity cannot be completely achieved without information on the topological (spatial) properties of the magnetic field. On the

contrary, information on the cross-helicity can be achieved in principle even with a single spacecraft measurement. This is the main reason why cross-helicity in solar wind turbulence is, in general, more deeply investigated than magnetic helicity. However, there exists a way to get information on a surrogate of H_m, even with measurements from a single spacecraft.

Statistical information about the magnetic helicity is derived from the Fourier transform of the magnetic field auto-correlation matrix $R_{ij}(\mathbf{r}) = \langle B_i(\mathbf{x}) \cdot B_j(\mathbf{x}+\mathbf{r})\rangle$ as shown by Matthaeus & Goldstein (1982). In other words, while the trace of the symmetric part of the spectral matrix accounts for the magnetic energy, the imaginary part of the spectral matrix accounts for the magnetic helicity (Batchelor 1970; Montgomery & Turner 1981; Matthaeus & Goldstein 1982). However, in situ measurements in space experiments really provide data from a single spacecraft. Consequently, we obtain values of R only for collinear sequences of $\mathbf{r}$ along the $\mathbf{x}$-direction, which corresponds, in the solar wind case, to the radial direction from the Sun. In these conditions, the Fourier transform of R allows us to obtain only a reduced spectral tensor along the radial direction so that $H_m(k)$ will depend only on the wavenumber k in this direction. Although the reduced spectral tensor does not carry the complete spectral information of the fluctuations, for slab and isotropic symmetries it contains all the information of the full tensor. Matthaeus & Goldstein (1982) provided the following simplified form to compute the reduced H_m for collinear measurements:

$$H_m^r(k) = \frac{2\,\mathrm{Im}[Y^*(k)\cdot Z(k)]}{k}, \tag{3}$$

where Y and Z are the Fourier coefficients of the components of the magnetic field B_y and B_z (both perpendicular to the sampling direction $\mathbf{x}$ along the radial direction), respectively, and $*$ indicates the complex conjugate. The first magnetic helicity spectra in the solar wind were shown by Matthaeus & Goldstein (1982), who analyzed *Voyager* data between 1 and 5 AU. They found that positive and negative helicity is randomly distributed across the spectrum so that the handedness of fluctuations at a given frequency is uncorrelated to the handedness of fluctuations at nearby frequencies. This alternating sign, especially at the smallest scales, causes the net magnetic helicity to be dominated by the largest scales, which are of the order of or larger than the magnetic correlation length, which is in agreement with the predictions of an inverse cascade and selective decay. The inverse cascade of H_m was first discussed by Frisch et al. (1975). In a turbulent process, while energy cascades from the injection scale to the much shorter dissipation scale, magnetic helicity undergoes an inverse cascade to lower wavenumbers, forming ordered force-free magnetic structures (see, for example, Dasso et al. 2005; Gulisano et al. 2005). In agreement with these theoretical predictions, Matthaeus & Goldstein (1982) attributed this large-scale behavior of magnetic helicity to the presence of large-scale flux tubes roughly aligned to the local Parker's spiral. Within each tube the longest wave fluctuations are not mirror symmetric, and the mean field might be interpreted as a helix with its axis along the Parker spiral direction. Neighboring flux tubes would have the same structure but different helicity content. Later, Goldstein et al. (1994) looked in detail at the properties of the fluctuating magnetic helicity in both the inertial and the so-called dissipation range. The analysis of the inertial range confirmed previous results obtained by Matthaeus & Goldstein (1982) but also pointed out that magnetic fluctuations contributing to the helicity were probably quasi-planar with minimum variance along the mean local field.

Thus, at least within the inertial range, a dominant magnetic helicity sign does not exist. However, we have to consider that these results refer to the frequency domain and provide averaged, say global, information on the magnetic helicity of the whole spatial range spanned by the spacecraft during the observational period. In other words, it could happen that spatial structures with a characteristic magnetic helicity sign might cross the spacecraft. This consideration prompts a search for alternative ways of computing reduced magnetic helicity in order to obtain the spatial evolution of this quantity and, by means of the Taylor's hypothesis (Taylor 1938), local information also relative to its behavior in the time domain.

A natural solution is using wavelet transform instead of Fourier transform, as first shown by Bruno et al. (2008) and later by He et al. (2011) and Podesta & Gary (2011). It is true that some improvements on the classical Fourier technique can be obtained using dynamic spectra (Goldstein et al. 1994), but the results are far from being as satisfactory as the ones we show in this paper, where we adopt this new technique based on wavelet decomposition much sharper than dynamic spectra, especially in terms of time resolutions.

In this paper, we test the performances of our technique on both synthetic and real data containing time intervals characterized by a dominant sign of magnetic helicity. In particular, these data refer to flux-rope events taken from a list of events reported by Feng et al. (2007) and observed by the *Wind* spacecraft.

Magnetic flux ropes are regions of twisted magnetic fields and can be described as a cluster of magnetic field lines bent into a tube-like shape with a strong axial field. The magnetic field far from the axis is weak and azimuthal (Russell & Elphic 1979). Flux ropes are a common phenomenon in the heliosphere, being observed in a variety of locations throughout the solar system, including the solar photosphere (e.g., Lites 2005; Mandrini et al. 2005), the solar wind (e.g., Burlaga et al. 1981; Moldwin et al. 1995), and in different locations of planetary magnetospheres and ionospheres (see Briggs et al. 2011 and references therein).

Small-scale solar wind flux ropes have recently been extensively studied at 1 AU (Feng et al. 2007, 2008; Cartwright & Moldwin 2008) and in the inner heliosphere (Cartwright & Moldwin 2010). The comprehensive surveys at 1 AU indicated a population of small-scale flux ropes that dominates in occurrence frequency over large-scale flux ropes (or magnetic clouds; MCs) identified from the Lepping et al. (2006) database. These structures differ from MCs in several aspects. Small-scale flux ropes have durations on the order of tens of minutes to several hours and scale sizes on the order of 0.01 AU, while MCs are on the order of tens of hours and a quarter of an AU in size. Small-scale flux ropes have constant temperature profiles similar to the surrounding solar wind, unlike MCs, which have depressed proton temperatures. These differences may be attributed to different origins of these structures, with MCs forming in the lower corona and small-scale flux ropes forming either locally in the solar wind or on the solar surface. However, this topic is still debated, as reported in the conclusions of this paper.

This paper is organized as follows: A description of the method and a numeric test are given in Section 2. The application of this technique on *Wind* data is provided in Section 3, followed by a discussion of the results and concluding remarks in Section 4.

2. METHOD DESCRIPTION AND NUMERIC TEST

The novelty of this paper is the study of reduced magnetic helicity and cross-helicity features of localized structures in

space plasma, investigated in both scale and time. As a matter of fact, using the wavelet transform (Torrence & Compo 1998), Equation (3) can be rewritten as

$$H_m^r(k,t) = \frac{2\,\mathrm{Im}[W_y^*(k,t)\cdot W_z(k,t)]}{k}, \quad (4)$$

where $W_y(k,t)$ and $W_z(k,t)$ are the wavelet transforms of the y- and z-components of the magnetic field. Equation (4) can also be written in its normalized form

$$\sigma_m(k,t) = \frac{k\,H_m(k,t)}{|W_y(k,t)|^2 + |W_z(k,t)|^2}, \quad (5)$$

where we dropped the suffix r for simplicity and where $|W_y(k,t)|$ and $|W_z(k,t)|$ are the moduli of the wavelet coefficients belonging to the complex wavelet transform of B_y and B_z. This parameter $\sigma_m(k,t)$ can vary between -1 and $+1$, indicating which is the dominating handedness. The use of the wavelet transforms in deriving the magnetic helicity can be applied, as we will see in the following, to the time localization of left- or right-handed flux ropes as well as to the identification of their characteristic timescales.

The wavelet function that is best suited to the data depends on the aim of the study. In choosing the wavelet function, there are several factors that are to be considered, such as whether it is complex or real valued, and its width. Complex wavelets, such as the Paul and Morlet functions, are ideal candidates for this study since they yield complex wavelet transforms that can be used to evaluate the magnetic helicity content of the flux ropes. Concerning the width of the wavelet function, it is worth noting that it is correlated to the resolution of the wavelet itself: A narrow (in time) function, such as the Paul wavelet, has good time resolution but poor frequency resolution, while a broad function, such as the Morlet wavelet, has poor time resolution but good frequency resolution. Since the main aim of this study is the investigation of the time behavior of reduced magnetic helicity, cross-helicity, and residual energy in space plasmas, rather than the different timescales involved, the Paul wavelet, which has a better time localization capability than the Morlet, has been used throughout the analysis shown in this paper.

Wavelet analysis can also be used to characterize the degree of alignment between magnetic and velocity fluctuations, already referred to as reduced cross-helicity, and allows us to rewrite Equation (2) as

$$H_c^r(k,t) = W^+(k,t) - W^-(k,t), \quad (6)$$

where $W^{\pm}(k,t)$ are the sum of the power of the wavelet transforms of the components of the Elsàsser variables $Z^{\pm}(t)$. These variables are defined as $Z^{\pm}(t) = V(t) \pm V_a(t)$, where $V_a(t) = \pm B/\sqrt{4\pi\rho}$ and the sign of this relation depends on the sign of $-\mathbf{k}\cdot\mathbf{B_0}$, ρ being the mass density and $\mathbf{B_0}$ being the average magnetic field. Thus, Z^+ and Z^- always indicate Alfvén waves moving away from or toward the Sun, respectively. Equation (6) can also be written in its normalized form

$$\sigma_c(k,t) = \frac{W^+(k,t) - W^-(k,t)}{W^+(k,t) + W^-(k,t)}. \quad (7)$$

Depending on the value of σ_c, we can infer whether the dominant modes are outward or inward directed. Finally, wavelet transform of velocity and magnetic field were used to compute the residual energy of the fluctuations as

$$E_r(k,t) = W_{\mathbf{kin}}(k,t) - W_b(k,t), \quad (8)$$

Table 1
Characteristics of the Synthetic Data Intervals Shown in Figure 1

Interval	H_m	H_c	E_r	t_c
1	>0	<0	0	150
2	<0	>0	<0	300
3	>0	<0	0	450
4	>0	>0	>0	150
5	<0	>0	0	300
6	>0	>0	<0	450

Note. Intervals are numbered from 1 to 6, moving from left to right, respectively. In terms of handedness, H_m, cross-helicity sign, H_c, residual energy sign, E_r, and timescale, t_c (in arbitrary units).

where $W_{\mathbf{kin}}(k,t)$ and $W_b(k,t)$ are the sum of the power of the wavelet transforms of the components of velocity $\mathbf{V}(t)$ and magnetic field $\mathbf{B}(t)$. This parameter is expected to fluctuate between positive and negative values depending on kinetic or magnetic energy dominance, respectively. In the case of Alfvénic fluctuations, this parameter should be zero because of energy equipartition. Similar to Equation (7), we can define the normalized residual energy as follows:

$$\sigma_r(k,t) = \frac{W_{\mathbf{kin}}(k,t) - W_b(k,t)}{W_{\mathbf{kin}}(k,t) + W_b(k,t)}. \quad (9)$$

This parameter varies between -1 and $+1$ depending on the dominance of kinetic or magnetic energy, respectively.

A first numeric test to show the reliability of our technique was performed on synthetic data simulating observations of the interplanetary magnetic field and plasma velocity. The synthetic data are given in the same referencer system used for *Wind* data, the analysis and results of which are presented in Section 3. The reference system is consistent with the Geocentric Solar Ecliptic (GSE) Cartesian coordinates: The x-axis points toward the Sun, so that at $x > 0$ one always observers a clockwise (counterclockwise) rotation in the y–z plane if the magnetic helicity is positive (negative). It turns out that it is possible to compare the sign of the magnetic helicity inferred from the synthetic data with that obtained from *Wind* data, namely, the same chirality of a helical structure leads to the same sign of the magnetic helicity in both synthetic and *Wind* data. The synthetic data set was derived by varying the direction of a vector of constant magnitude around the x-axis to obtain intervals of defined magnetic helicity, either positive or negative. In a similar way, a second vector, representing the velocity vector, fluctuated in phase or in counterphase with respect to the magnetic vector in order to simulate either positive or negative cross-helicity. In addition, different time intervals were characterized by a different kinetic to magnetic energy ratio in order to simulate cases of either magnetic or kinetic energy dominance along with cases of energy equipartition. For the sake of clarity, these different time intervals were separated by shorter samples of white noise. The amplitudes of the y- and z-components were kept constant in all intervals except the first and third ones to allow some time dependence of magnetic helicity as shown in Figure 1.

The left side of Figure 1 shows, from top to bottom, the time profile of the three magnetic field components and the vector intensity, respectively. The right side shows the hodogram for the two perpendicular components as function of time. In summary, six time intervals characterized by different magnetic helicity, cross-helicity, and residual energy were generated at different scales as summarized in Table 1. The sign of magnetic helicity was defined as negative for left-hand or counterclockwise

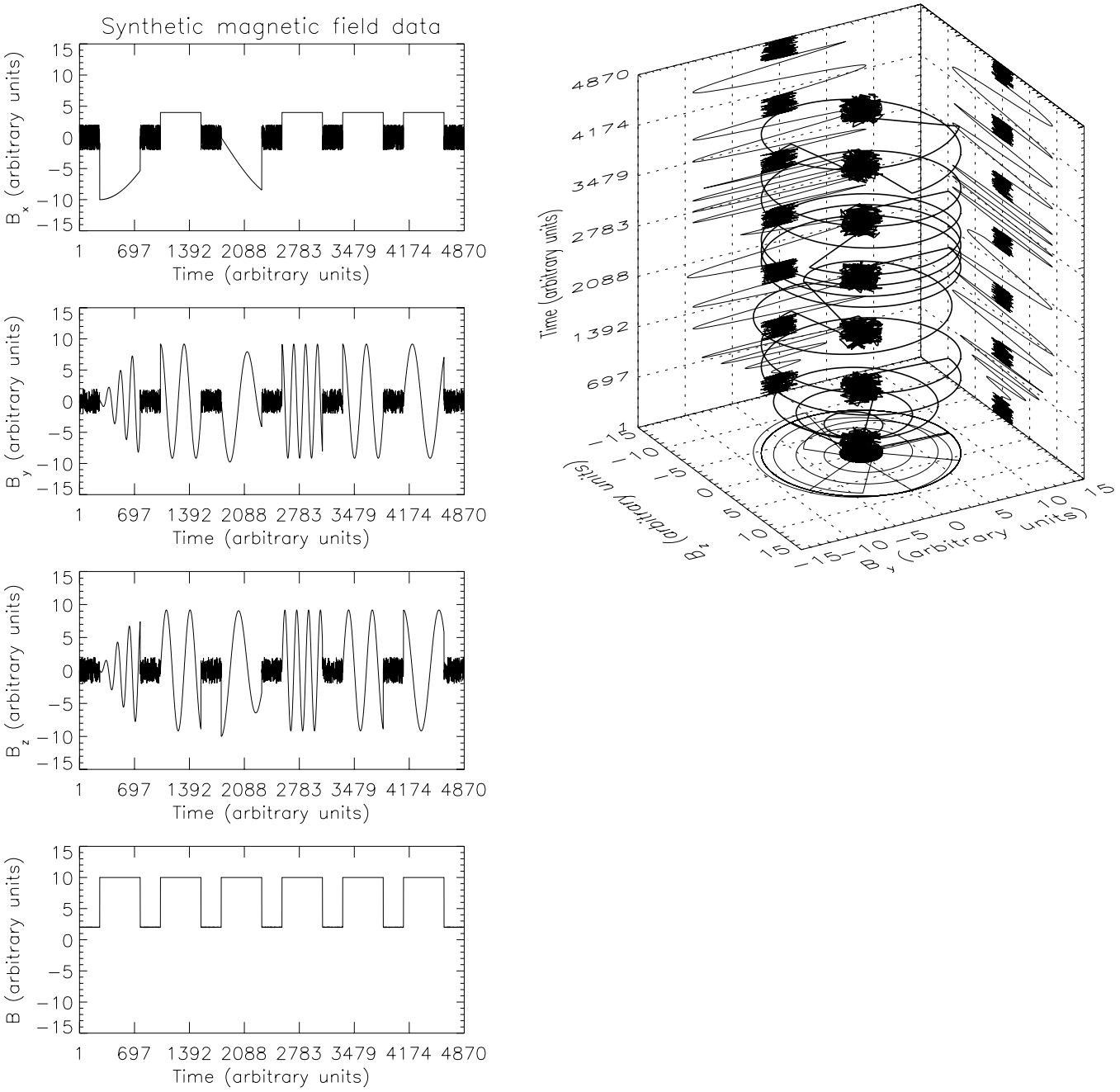

Figure 1. Left: from top to bottom, time profiles of synthetic magnetic field components B_x, B_y, B_z, and vector magnitude B, respectively. The amplitudes of the y- and z-components were kept constant in all intervals except the first and third ones to allow some time dependence of magnetic helicity. Right: hodogram of the fluctuating y- and z-components as a function of time, along with the projections on the three associated planes.

rotation of the magnetic vector on the plane perpendicular to the sampling direction, while the positive sign was attributed to clockwise or right-hand field rotation.

Figure 2 shows the results of this technique applied to synthetic data and limited to magnetic helicity computation. The top panel of Figure 2 displays the time profile of the two perpendicular magnetic components B_y and B_z used to compute magnetic helicity. Short white noise intervals are clearly distinguishable.

From the results of the wavelet magnetic helicity spectral analysis performed on the B_y and B_z components and shown in the scalogram in the bottom panel, it is possible to identify the scale of the magnetic helicity events, indicated by the smallest contour inside each colored island, the handedness or magnetic helicity sign, and the starting and ending times of each event (compared to data reported in Table 1). It can be noticed that determination of the scale by means of the Paul wavelet introduces some uncertainty, as already anticipated, due to the nature of this wavelet basis. However, the time duration of each island inferred from the $1/e$ width is in agreement with the expected one (512 data points) within a 10% error. On the other hand, the uncertainty introduced in scale determination can be estimated to be within $\sim$15% of the expected scale length, which is reported in Table 1. The cross-hatched area in Figure 2 corresponds to the Cone of Influence (COI), which indicates the regions in which edge effects, due to finite-length time series, become important. Features below this line (i.e., at longer scales) are not fully reliable.

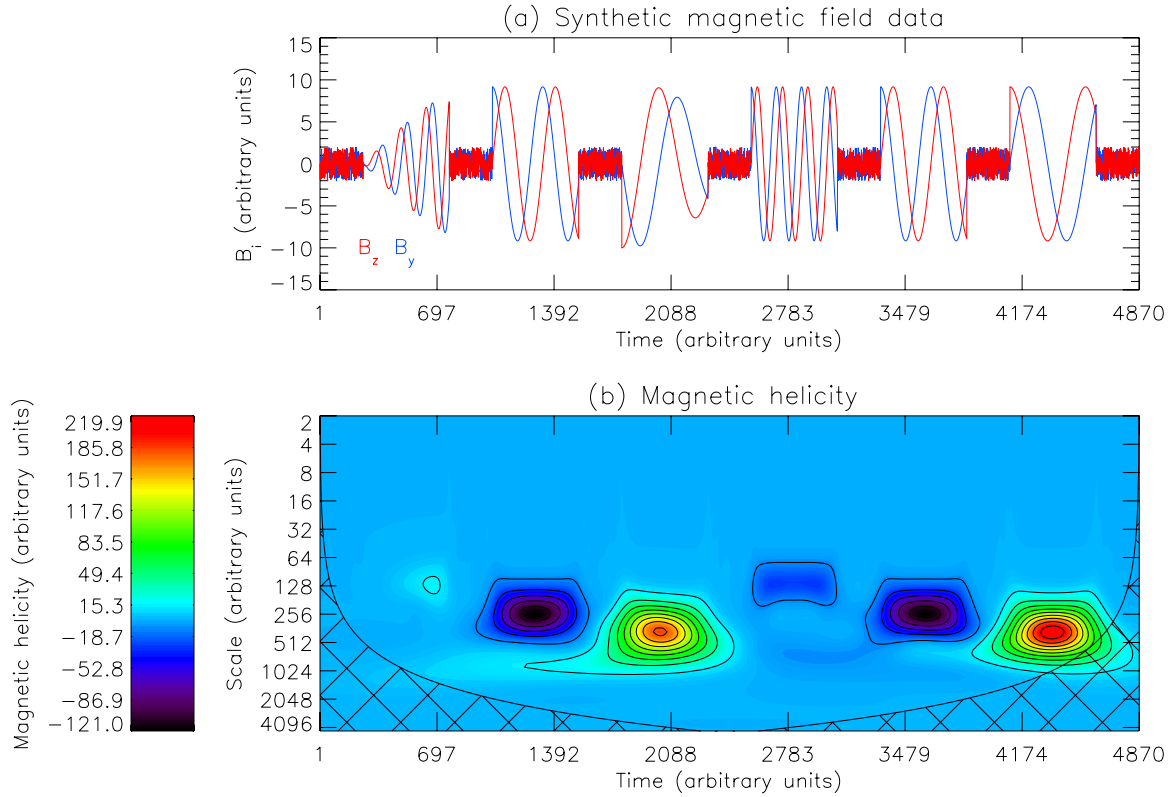

Figure 2. Top panel: B_y and B_z (blue and red curves, respectively) components of the synthetic magnetic field data. Bottom panel: wavelet magnetic helicity spectrum using the Paul wavelet function; the cross-hatched area marks the COI where edge effects become important.
(A color version of this figure is available in the online journal.)

Results of cross-helicity and residual energy analysis are shown in Figure 3. Panel (a) shows the time profile of the components of the synthetic velocity and magnetic field data. Panel (b) shows the scalogram relative to cross-helicity. Also in this case, as for magnetic helicity analysis, the wavelet technique we adopted returns the correct cross-helicity sign for each of the time intervals defined in Table 1. Panel (c) shows results relative to residual energy computation. Also in this case, these results fully agree with the expected sign for the residual energy since only intervals numbered 2, 4, and 6 are not characterized by magnetic and kinetic energy equipartition. These results on synthetic data made us confident of the validity of this technique, which we have successively applied to two case studies of interplanetary flux ropes in order to characterize them in terms of magnetic helicity, cross-helicity, and residual energy scale by scale. To our knowledge, this is the first time this kind of study has been performed on interplanetary flux ropes; in the future, it could be extended to MCs.

3. *WIND* OBSERVATIONS OF FLUX ROPES

Interplanetary magnetic flux ropes (IMFRs) were selected from the database by Feng et al. (2007), who identified more than one hundred such objects by an enhanced magnetic field strength and the rotation of the magnetic field direction. Typically, the length scale of those events is about 0.05 AU or smaller, and their duration is from one to several hours. The two events studied in the present paper are listed along with their dimensions and durations in Table 2.

The analyzed data were taken from the Magnetic Field Investigation (MFI) instrument (Lepping et al. 1995) on board *Wind* with a 3 s resolution for the computation of magnetic helicity.

Table 2
Beginning and End of the Two Interplanetary Flux Ropes

Start Date hh:mm	End Date hh:mm	Δt (hr)	D (AU)
1997 May 24 02:22	1997 May 24 07:30	5.13	0.037
1998 Mar 28 22:47	1998 Mar 29 02:11	3.40	0.043

Note. Duration of the event, Δt, in hr, diameter of the flux rope, D, in AU (as reported in Feng et al. 2007).

The cross-helicity and the residual energy were computed using 60 s averaged coming from the OMNI database. During the selected time periods, averages data from the *Wind*/MFI instrument for magnetic field components and from the Solar Wind Experiment instrument (Ogilvie et al. 1995) on board *Wind* for velocity components and number density were used.

The time intervals under study are shown in Figures 4 and 5; they comprise 40 and 23 hr, respectively, centered at the time when the event took place. The left side of each figure shows the time series of the magnetic field components and magnitude in the GSE Cartesian coordinates. The events identified by Feng et al. (2007) are delimited by dashed vertical lines. On the right side of each figure, a three-dimensional hodogram showing the time series of the y- and z-components of the magnetic field and their relative projection on the y–z plane, perpendicular to the sampling direction x reveals a counterclockwise rotation (i.e., negative handedness) for the event shown in Figure 4 and a clockwise rotation (i.e., positive handedness) for the event shown in Figure 5 in the reference system introduced in Section 2. There is not necessarily a correspondence with the

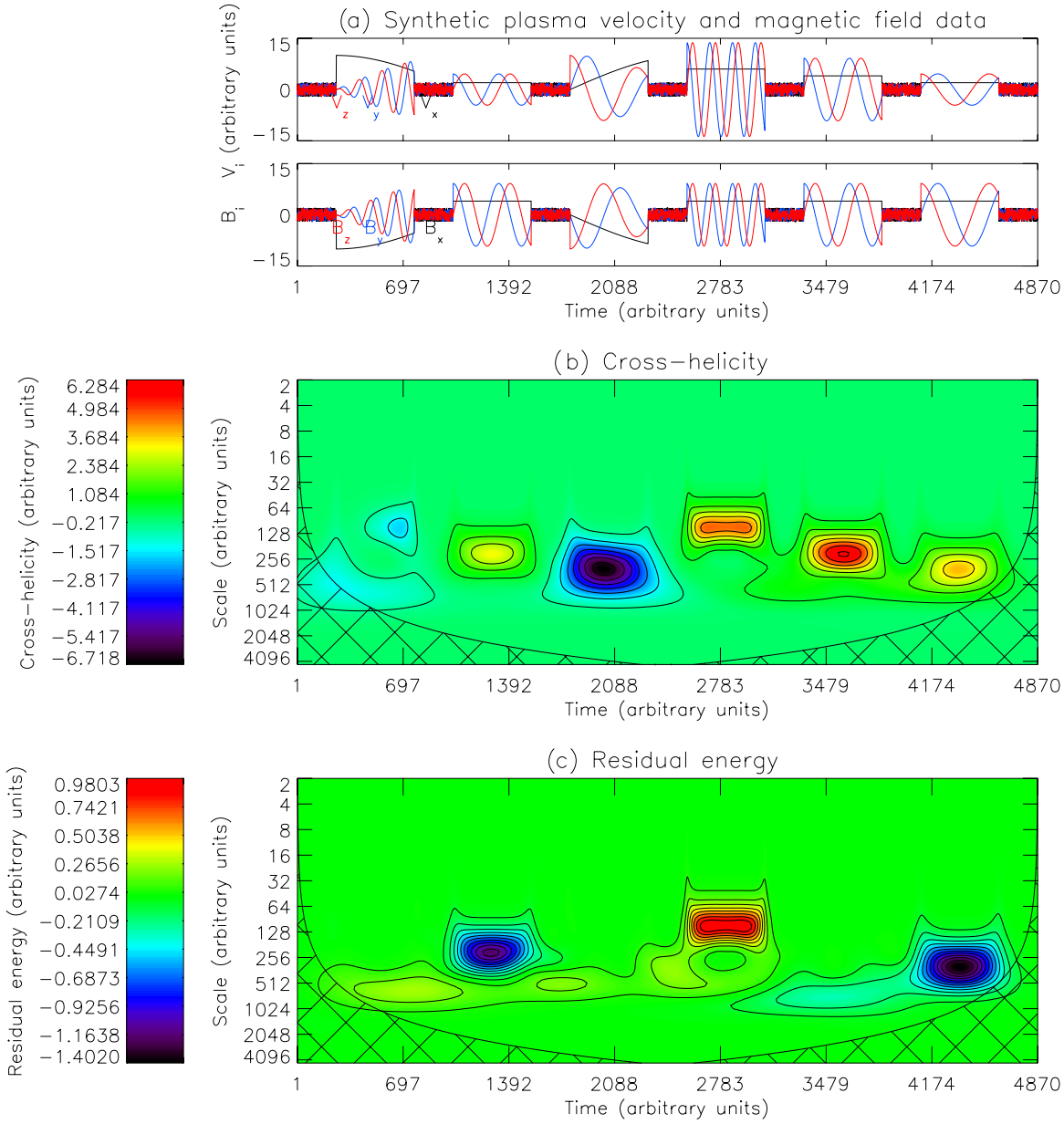

Figure 3. (a) Time profile of V_x (black curve), V_y (blue curve), and V_z (red curve) components of the synthetic velocity data (top panel). (a) Time profile of B_x, B_y, and B_z components of the synthetic magnetic field data in the same format as of velocity data (bottom panel). (b) Cross-helicity islands identified by the technique described in the text. Color scale indicates cross-helicity value. The sign of each island agrees with indications given in Table 1. (c) Residual energy results indicate that only three islands are out of equipartition as indicated in Table 1. The first and third islands show an excess of magnetic energy, while the second one shows an excess of kinetic energy.

(A color version of this figure is available in the online journal.)

intrinsic chirality of the interplanetary flux ropes. In particular, the first event of 1997 May was embedded in a slow wind region, while the second event of 1998 March happened to be close to the border between two regions characterized by different wind speed.

The analysis of the magnetic helicity in the solar wind allows the study of how the magnetic field is sheared or twisted compared to its lowest energy state (potential field), and it is particularly apt to identify interplanetary flux ropes.

For the reader's ease, we decided to indicate scales as a time (in hr) for better comparison with the results by Feng et al. (2007). By virtue of Taylor's hypothesis (Taylor 1938), the shift from the k-domain to the time domain was obtained by dividing for 2π and multiplying for the average value of the solar wind speed during the two time intervals, namely, 303 and 456 km s^{-1}, respectively. The long uninterrupted *Wind* data set and the short sampling time $\Delta t = 3$ s allow the investigation of the characteristic timescales of the interplanetary flux ropes from $T_{\rm NS} = 2 \cdot \Delta t = 6$ s, the Nyquist–Shannon timescale, up to several hours.

Since the magnetic helicity density spectrum is quite steep with a spectral index around $-8/3$, as we verified on the basis of a magnetic helicity spectral density computed via a fast Fourier transform on the same data set (see also determinations by Bruno & Dobrowolny 1986 in the inner heliosphere around 1 AU and by Matthaeus & Goldstein 1982 in the outer heliosphere), we

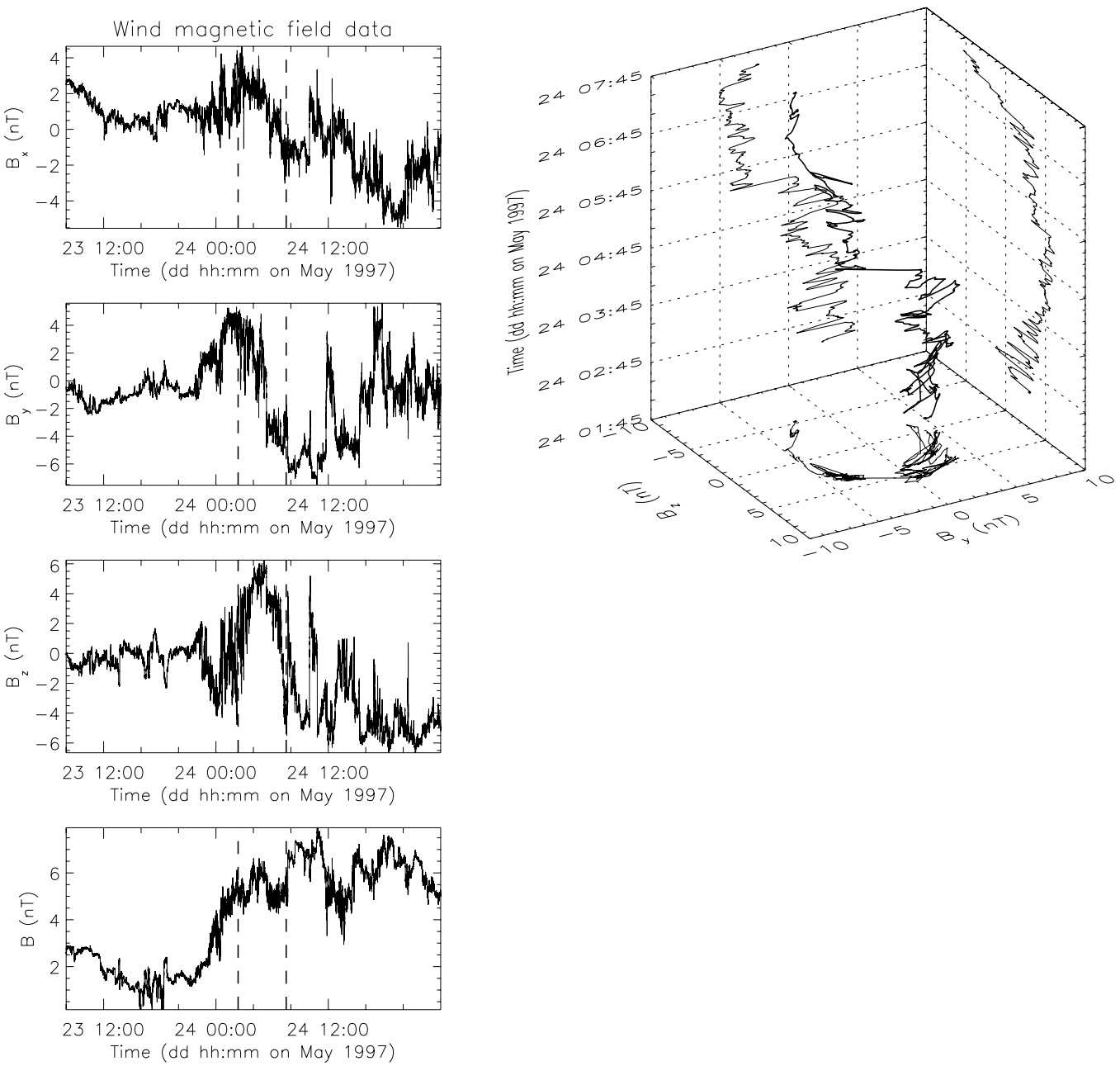

Figure 4. Left: from bottom to top, magnetic field components and magnitude in the GSE Cartesian coordinates of the IMFR occurred on 1997 May 24. The event identified by Feng et al. (2007) is delimited by dashed vertical lines. Right: three-dimensional hodogram of the y and z magnetic field components as a function of time along with the projections on the three associated planes. This plot has been smoothed with a 31 points running window to allow for a better view.

chose to compensate magnetic helicity scalogram as resulting from our wavelet analysis multiplying $H_m^r(f,t)$ by $f^{8/3}$. In doing so, we are also able to show helicity structures at scales much smaller than the main helicity event represented by the flux rope.

Figure 6 refers to a time interval containing the flux-rope event of 1997 May 24 spotted by Feng et al. (2007). The top panel shows the time profile of the two components of the magnetic field, B_y and B_z, perpendicular to the sampling direction x; the flux-rope event is identified by the two vertical dashed lines. Magnetic field fluctuations appear to be of much larger amplitude in the downstream region with respect to the flux rope. The bottom panel shows the compensated magnetic helicity scalogram up to scales around 32 hr. Magnetic helicity values $H_m^r(f,t)$ have been multiplied by $|\sigma_m(f,t)|$ in order to highlight the best helicity cases. A large twisted flux rope is clearly identified in the middle of the panel. Its helical structure seems to be limited to scales around approximately 5 hr, in agreement with Feng's evaluation reported in Table 2, and no helical structures are observed at smaller scales within the flux rope, indicating that magnetic field lines are twisted at fairly constant pace throughout the helical structure. On the contrary, the presence of a tail as we move farther out from the flux rope and including larger scales can be ascribed to a larger helical structure, presumably an MC occurring about 6 hr later the end of the flux rope as reported in Feng's database. Minor helical structures with opposite helicity can be observed sporadically at smaller scales and at different times with respect to the flux rope.

Figure 7 shows a time interval containing the flux-rope event of 1998 March 28 (Feng et al. 2007). In this case the helical wrapping of magnetic field lines seems not to be limited to a

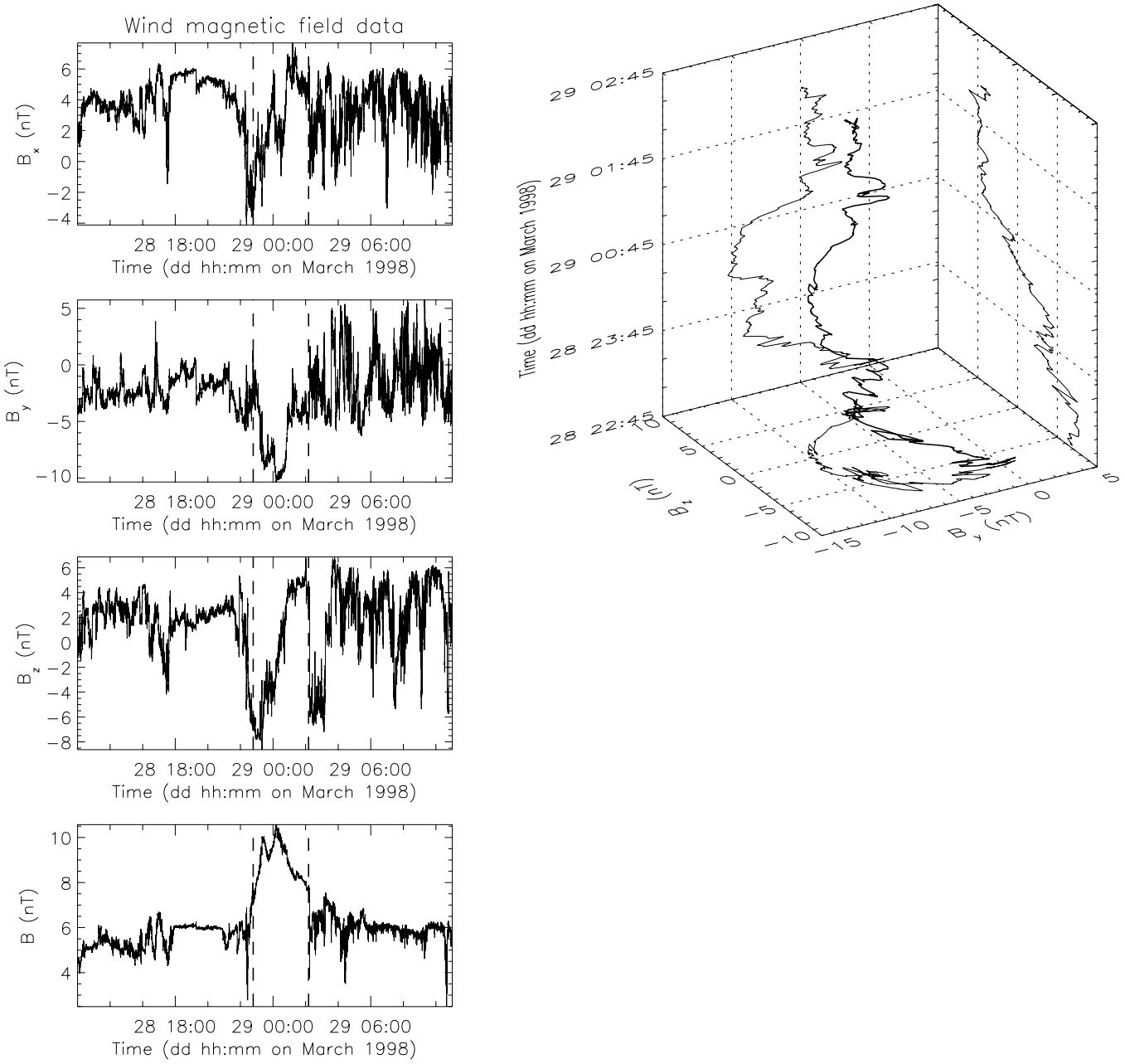

Figure 5. Same as Figure 4, but for the IMFR event occurred on 1998 March 28.

narrow range of scales around 3 hr, as Table 2 suggests, but contour lines show that also smaller scales within the flux rope show helicity features. Again, this structure seems to be at the border between two regions characterized by different levels of magnetic fluctuations. As a matter of fact, this helical event separates a slow wind region from a region that is characterized by a faster bulk speed and quite is also Alfvénic, as will be discussed later. Even in this case, the downstream region is populated by a certain number of smaller scale structures whose magnetic field possesses some helical property. So, as in the previous case, the presence of helical structures seems to be related to regions of enhanced magnetic field fluctuations which, in this particular case, are also Alfvénic.

Figure 8 shows cross-helicity results relative to the flux-rope event of 1997 May 24. The time profiles of velocity component fluctuations and magnetic field components in Alfvén units are shown in the top panels, where the vertical dashed lines identify the location of the flux rope. Panel (b) shows the scalogram relative to the cross-helicity analysis. Analogously to what was done for magnetic helicity values, original cross-helicity values have been compensated by a factor of $f^{5/3}$ to highlight the behavior of this quantity at small scales. This value was evaluated fitting the corresponding power density spectrum (see also Matthaeus & Goldstein 1982). Moreover, cross-helicity values $H_c^r(f, t)$ have been multiplied by $|\sigma_c(f, t)|$ to highlight the best cross-helicity events. There is a general low level of cross-helicity throughout the time interval, with exceptions made for the flux rope and shorter time intervals distributed along the whole duration of the data sample at smaller scales. Cross-helicity in the flux rope is positive and shows some smaller cross-helicity structure of alternate sign at smaller scales. However, there is not a general trend of

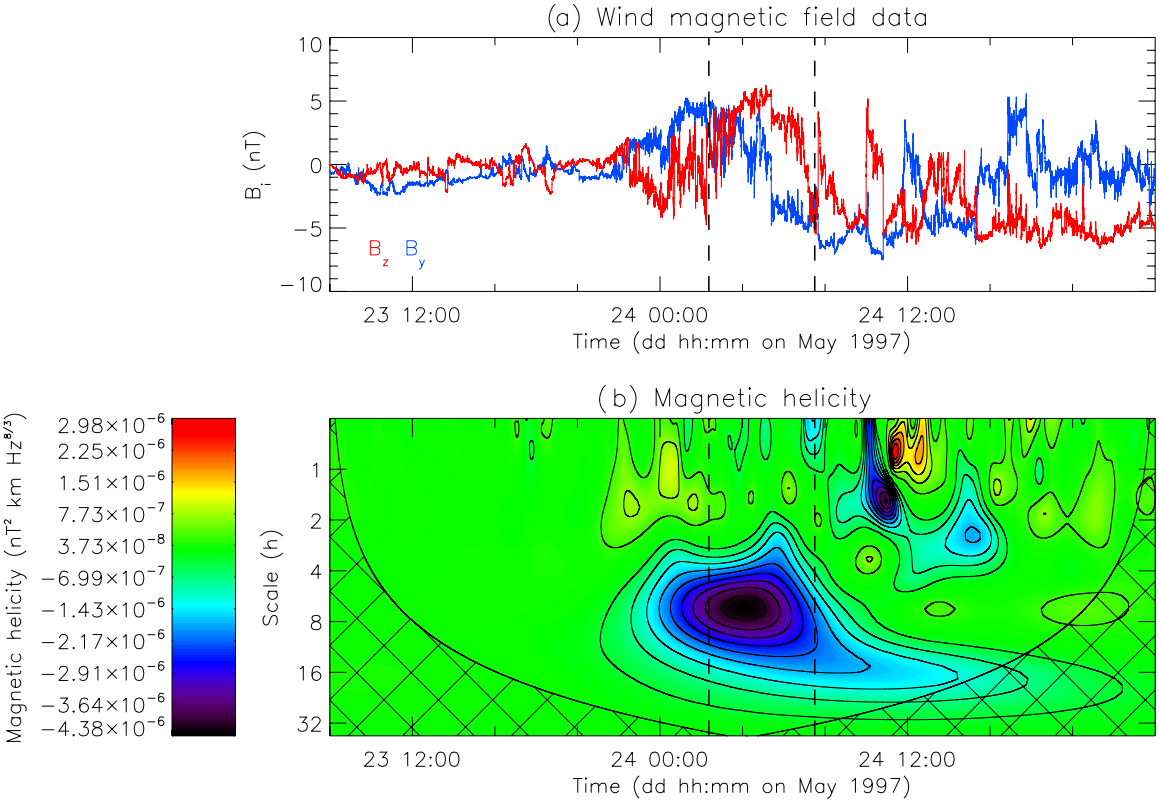

Figure 6. Top panel: magnetic field time series acquired by *Wind* during the passage of the flux rope on 1997 May 24. The black and red curves represent the y- and z-components, respectively; the event identified by Feng et al. (2007) is delimited by dashed vertical lines. Bottom panel: scalogram of magnetic helicity $H_m^r(f,t)$ multiplied by $|\sigma_m(f,t)|\cdot\mathbf{f^{8/3}}$, using the Paul mother wavelet; the cross-hatched area marks the COI where edge effects become important.
(A color version of this figure is available in the online journal.)

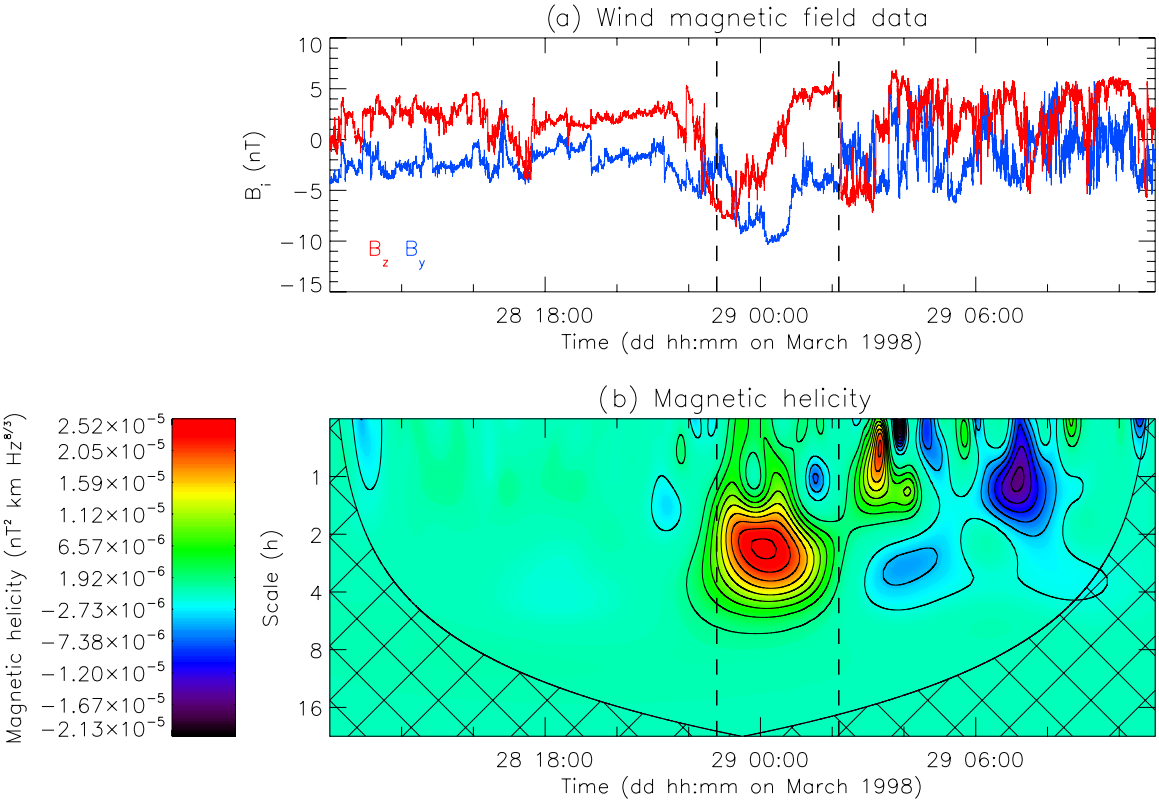

Figure 7. Same as Figure 6, but for the IMFR event that occurred on 1998 March 28.
(A color version of this figure is available in the online journal.)

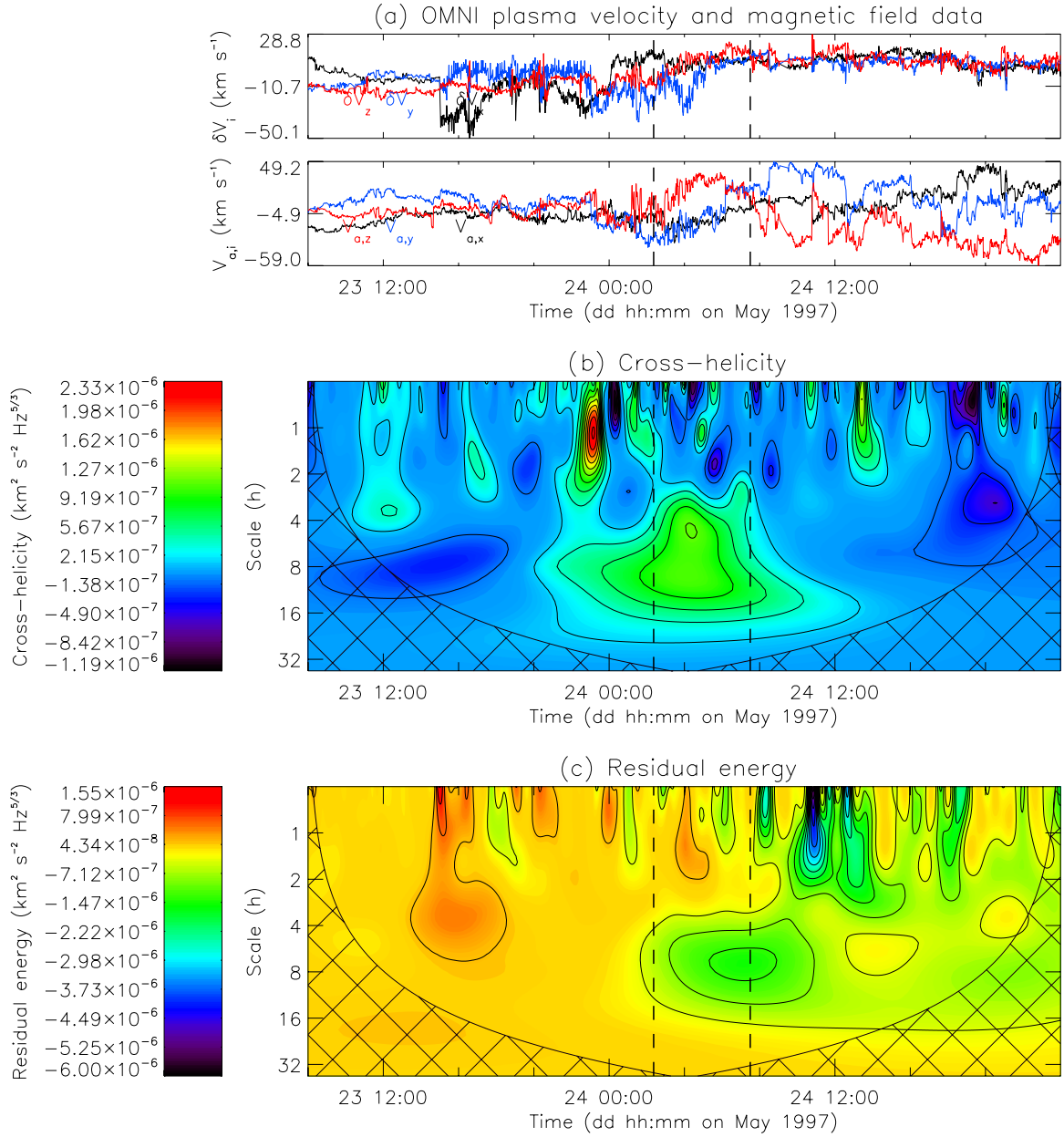

Figure 8. Flux rope of 1997 May 24. (a) Time profiles of velocity fluctuations and magnetic field in Alfvén units. (b) Scalogram of cross-helicity $H_c^r(f,t)$ multiplied by $|\sigma_c(f,t)|\cdot\mathbf{f^{5/3}}$. (c) Scalogram of the residual energy $E_r^r(f,t)$ multiplied by $|\sigma_r(f,t)|\cdot\mathbf{f^{5/3}}$.
(A color version of this figure is available in the online journal.)

cross-helicity throughout the time interval. Panel (c) shows the residual energy scalogram compensated by a factor of $f^{5/3}$ and multiplied by $|\sigma_r(f,t)|$ (same considerations applied for cross-helicity). This quantity is generally around zero within the upstream region with respect to the flux rope, with exceptions made for a few spots where the kinetic energy slightly prevails on the magnetic counterpart. On the other hand, within the flux rope and generally in the downstream region, where magnetic fluctuations are enhanced, magnetic energy overcomes kinetic energy. Within the flux rope, at smaller scales, there is not a clear trend.

Figure 9 shows results relative to the flux-rope event of 1998 March 28. Also in this case, as already previously noticed, magnetic field fluctuations are of much larger amplitudes compared to the upstream region, but, in addition, cross-helicity results also show that they are correlated to velocity fluctuations and that these Alfvénic correlations are outward directed. The flux rope shows a lower level of cross-helicity compared to the downstream region but, unlike the previous flux rope, the cross-helicity sign agrees well with the general sign within the downstream region, suggesting some common origin between this flux rope and the downstream region. In practice, the situation is opposite that discussed for the previous flux rope, where its cross and magnetic helicity seem not to be connected to the surrounding plasma region. In addition, panel (c) shows that these fluctuations are characterized by a better energy equipartition, typical of Alfvénic fluctuations, as we move farther out from the flux rope into the downstream

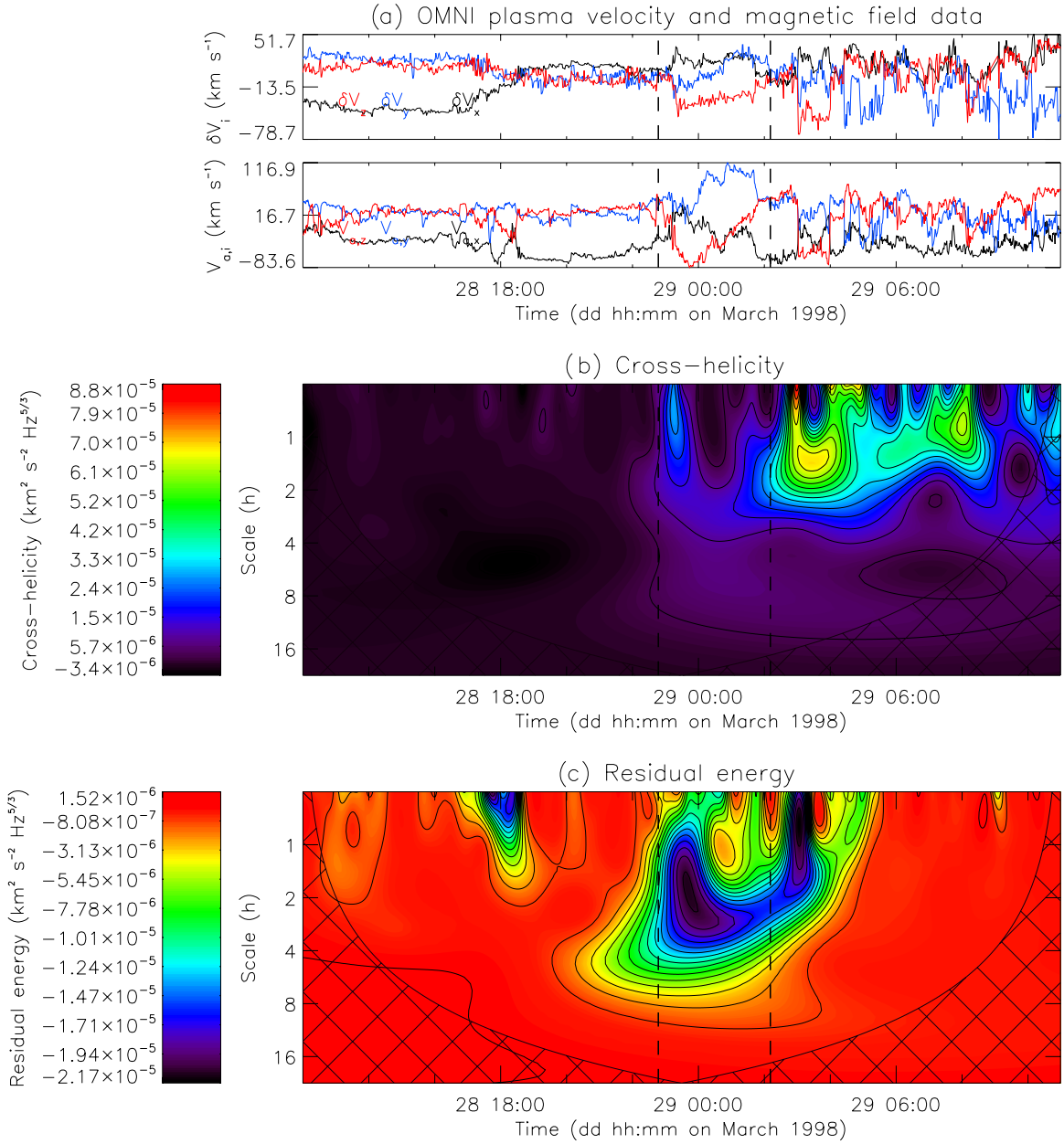

Figure 9. Same as Figure 8, but for the IMFR event that occurred on 1998 March 28.
(A color version of this figure is available in the online journal.)

region. On the other hand, similar to the previous case, the flux rope shows a clear magnetic energy excess that in this case extends also to smaller scales within the flux rope.

4. SUMMARY AND CONCLUSIONS

In this paper, we adopted the use of the wavelet transform as a new tool to investigate the time behavior of different scales of reduced magnetic helicity, as first suggested by Bruno et al. (2008), but also of cross-helicity and residual energy in space plasma. The main goal was a better characterization of the fluctuations in which interplanetary flux ropes are embedded. Fluctuations inside interplanetary flux ropes already have been studied both theoretically (e.g., Dasso et al. 2003) and from observations (e.g., Leamon et al. 1998). However, our tool can represent the basis for a new treatment of in situ measurements of these quantities. In particular, we focused on two time intervals from the *Wind* spacecraft containing two flux ropes of opposite handedness and embedded into two different plasma regions, as identified by Feng et al. (2007).

The main results of our study can be summarized as follows: (1) Both flux ropes are located at the border between regions characterized by different levels of magnetic field fluctuations, the downstream region being characterized by much larger fluctuations with respect to the upstream one. A similar comment also applies to velocity fluctuations only for the second flux rope since the region that follows the rope is highly Alfvénic. Moreover, the second flux rope shows the same cross-helicity sign of the downstream region, while cross-helicity features of the first flux rope seem to be limited to the rope itself. (2) Both flux ropes, as expected, are characterized by a strong signature of magnetic helicity within a limited range of scales, but for the flux rope embedded in the region characterized by Alfvénic fluctuations the helical magnetic structures also extend to smaller scales.

(3) As expected, both flux ropes are magnetically dominated, but only for the second flux rope does this feature also extend to scales smaller than the main scale characterizing the structure.

From the above considerations it seems that the case studies analyzed in this paper would suggest different origins for the two different flux ropes advected by the solar wind. There is a debate as to where small-scale flux ropes originate. On one hand, they are suggested to be formed through magnetic reconnection in the solar wind such as across the heliospheric current sheet (e.g., Moldwin et al. 1995, 2000; Cartwright & Moldwin 2010). On the other hand, Feng et al. (2007, 2008) stated that they form in the corona, similar to MCs. Cartwright & Moldwin (2010) believe that there are two populations, one originating in the solar wind via magnetic reconnection across the current sheet in the inner heliosphere and the other originating in the corona. The latter suggested the interpretation of small-scale flux ropes as remnants of the streamer belt blobs formed from disconnection (Wang et al. 1998). However, at present no one-to-one observation of a blob and a small-scale flux rope in the solar wind has been found.

In both flux ropes studied in this paper, these advected structures are formed at the border between regions characterized by quite different levels of magnetic fluctuations, thus suggesting a possible role of turbulence in the generation process. In the 1997 May event, the flux ropes do not seem to share common magnetic helicity features with smaller scales or common cross-helicity features with the surrounding plasma region: the rope looks like a large-scale sheared magnetic structure. This should imply that it could have been generated through a process involving turbulent reconnection and subsequent generation of the magnetic structures at large scales. This might have happened at the Sun with successive advection by the wind, or it might have been generated locally. In the 1997 May event, the flux rope is characterized by correlated fluctuations of the magnetic field and velocity ($H_c > 0$), though the system is very far from equipartition ($E_r < 0$). This physical state is predicted by MHD equations, which have two non-trivial fixed points, namely: (1) an "Alfvénic state," which requires equipartition and alignment (anti-alignment) between velocity and magnetic fluctuations, and (2) a fixed point where the velocity is zero and the magnetic field is force-free. Both fixed points are exclusive: if one of them is satisfied, the other cannot be satisfied. A third fixed point can be recognized, namely, a state where velocity and magnetic fluctuations are correlated to a certain degree C, and (at the same time) the curl of the magnetic fluctuations is aligned (to a certain degree depending on the value of C) to the magnetic fluctuation itself. This fixed point does not require equipartition (Ting et al. 1986). The attractor basin of the third fixed point is much wider than the other. Then, in a decay situation, the MHD system will probably tend toward a state given by the third fixed point. Our analysis of the flux rope suggests that this third situation is actually observed in the 1997 May event.

The 1998 March event, on the contrary, looks different. The rope shares common physical characteristics with the downstream plasma where a region with a higher level of cross-helicity of the same sign is present. In this case, this would suggest a local generation of the flux rope, for example, through a relaxation process with different decays for energy and magnetic helicity, or an inverse cascade of helicity in the turbulent MHD environment. In fact a solution with a maximal magnetic helicity and zero cross-helicity can be obtained easily from MHD equations through a variational principle (Ting et al. 1986; Carbone & Veltri 1992). Recognizing these kinds of structures in the solar wind should be very interesting from a theoretical point of view because relaxation processes leading to large-scale magnetic field are usually observed in laboratory plasmas where rigid boundaries are present. On the contrary, free space plasma was believed to be characterized by dynamic alignment between velocity and the magnetic field (Carbone & Veltri 1992), namely, a state of maximal cross-helicity. In the case, we perhaps studied the border between two different plasma regions characterized by different cross-helicity and magnetic energy levels, which might represent a sort of "wall" within which relaxation processes can take place.

However, these considerations are based only on two case studies; we plan in the next future to increase the number of case studies to give statistical support to our conclusions.

This work was supported by the Italian Space Agency (ASI) Grants (I/023/09/0) and (I/015/07/0).

REFERENCES

Batchelor, G. K. 1970, Theory of Homogeneous Turbulence (Cambridge: Cambridge Univ. Press)
Briggs, J. A., Brain, D. A., Cartwright, M. L., Eastwood, J. P., & Halekas, J. S. 2011, Planet. Space Sci., 59, 1498
Bruno, R., & Carbone, V. 2005, Living Rev. Sol. Phys., 2, 4
Bruno, R., & Dobrowolny, M. 1986, Ann. Geophys., 4, 17
Bruno, R., et al. 2008, AGU Fall Meeting 2008, SH42A-06
Burlaga, L., Sittler, E., Mariani, F., & Schwenn, R. 1981, J. Geophys. Res., 86, 6673
Carbone, V., & Veltri, P. 1992, A&A, 259, 359
Cartwright, M. L., & Moldwin, M. B. 2008, J. Geophys. Res., 113, A09105
Cartwright, M. L., & Moldwin, M. B. 2010, J. Geophys. Res., 115, A08102
Dasso, S., Gratton, F. T., & Farrugia, C. J. 2003, J. Geophys. Res., 108, 1149
Dasso, S., Mandrini, C. H., Démoulin, P., Luoni, M. L., & Gulisano, A. M. 2005, Adv. Space Res., 35, 711
Dobrowolny, M., Mangeney, A., & Veltri, P. 1980, Phys. Rev. Lett., 45, 144
Feng, H. Q., Wu, D. J., & Chao, J. K. 2007, J. Geophys. Res., 112, A02102
Feng, H. Q., Wu, D. J., Lin, C. C., et al. 2008, J. Geophys. Res., 113, A12105
Frisch, U., Pouquet, A., Leorat, J., & Mazure, A. 1975, J. Fluid Mech., 68, 769
Goldstein, M. L., Roberts, D. A., & Fitch, C. A. 1994, J. Geophys. Res., 99, 11519
Gulisano, A. M., Dasso, S., Mandrini, C. H., & Démoulin, P. 2005, J. Atmos. Terr. Phys., 67, 1761
He, J., Marsch, E., Tu, C., Yao, S., & Tian, H. 2011, ApJ, 731, 85
Leamon, R. J., Smith, C. W., & Ness, N. F. 1998, Geophys. Res. Lett., 25, 2505
Lepping, R. P., Acũna, M. H., Burlaga, L. F., et al. 1995, Space Sci. Rev., 71, 207
Lepping, R. P., Berdichevsky, D. B., Wu, C.-C., et al. 2006, Ann. Geophys., 24, 215
Lites, B. W. 2005, ApJ, 622, 1275
Mandrini, C. H., Pohjolainen, S., Dasso, S., et al. 2005, A&A, 434, 725
Matthaeus, W. H., & Goldstein, M. L. 1982, J. Geophys. Res., 87, 6011
Matthaeus, W. H., Weygand, J. M., Chuychai, P., et al. 2008, ApJ, 678, L141
Moffat, H. K. 1978, Magnetic Field Generation in Electrically Conducting Fluids (Cambridge: Cambridge Univ. Press)
Moldwin, M. B., Ford, S., Lepping, R., Slavin, J., & Szabo, A. 2000, Geophys. Res. Lett., 27, 57
Moldwin, M. B., Phillips, J. L., Gosling, J. T., et al. 1995, J. Geophys. Res., 100, 19903
Montgomery, D., & Turner, L. 1981, Phys. Fluids, 24, 825
Ogilvie, K. W., Chornay, D. J., Fritzenreiter, R. J., et al. 1995, Space Sci. Rev., 71, 55
Podesta, J. J., & Gary, S. P. 2011, ApJ, 734, 15
Russell, C. T., & Elphic, R. C. 1979, Nature, 279, 616
Taylor, G. I. 1938, Proc. R. Soc. London A, 164, 476
Taylor, J. B. 1974, Phys. Rev. Lett., 33, 1139
Ting, A. C., Montgomery, D., & Matthaeus, W. H. 1986, Phys. Fluids, 29, 3261
Torrence, C., & Compo, G. P. 1998, Bull. Am. Meteorol. Soc., 79, 61
Wang, Y.-M., Sheeley, N. R., Jr., Walters, J. H., et al. 1998, ApJ, 498, L165
Woltjer, L. 1958, Proc. Natl Acad. Sci. USA, 44, 489